Journal of Hydraulic Structures
J. Hydraul. Struct., 2022: 8(2):1-13
DOI: 10.22055/JHS.2022.41051.1215

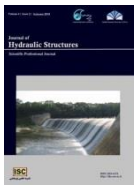

OPEN ACCESS

Experimental study on the removal of phenol from wastewater using Ni-doped ZIF-8 adsorbent; Isotherm models and operating conditions

Mehdi Sedighi [1]

Abstract

Phenols are considered serious contaminants because even at low concentrations, they are toxic and characteristics due to their toxic and carcinogenic properties. Removing the phenols from industrial effluents water before entering a stream is highly recommended Ni/ZIF-8 was used in a batch process to adsorb phenol from aqueous solutions at different temperatures. The operating conditions were considered as temperature, contact time, and initial pollutant concentration. The adsorption isotherms at different temperatures were determined based on three different models. For temperature range 25–40 ºC, the best-fitting adsorption isotherm models were Freundlich > Langmiur > Temkin. It was found that the Langmuir model fits the experimental data well, with maximum adsorption capacities of 36.8 mg/g at 25, 25.9 mg/g at 40 and 22.4 mg/g at 60 °C. According to the results of thermodynamic analysis, the adsorption of phenol onto zeolite is physical and exothermic. The Ni/ZIF-8 adsorbent proved to be effective in removing phenol by adsorption.

Keywords: Phenol removal, MOF, Adsorption Isotherm, Adsorption Capacity.

Received: 7 June 2022; Accepted: 9 July 2022

1. Introduction

Paint, polymeric pesticides, coal conversion, resins, petroleum and introducing petrochemical industries contribute the largest amount of phenol pollution to the aquatic environment [1]. Degradation of phenols or release of these substances into the environment refers to the presence of derivatives. Phenols are considered serious contaminants because even at low concentrations, they are toxic and characteristics [2, 3] due to their toxic and carcinogenic properties. Phenol is used as a disinfectant, reagent in chemical analysis, and in the manufacture of dyes, resins and medical and industrial organic compounds. Furthermore, it is used in the production of fertilisers, explosives, paints and paint removers as well as drugs, pharmaceuticals, textiles, and coke. It is produced in large quantities as an intermediate in the production of other chemicals.

In the construction, automotive, and appliance industries, phenol is used as an intermediate in

[1] Department of Chemical Engineering, University of Qom, Qom, Iran. E-mail: sedighi@qom.ac.ir

the manufacturing of phenolic resins, which are lightweight, low-cost thermoset resins. It is also used to produce caprolactam, which is used to make nylon and other synthetic fibres, and bisphenol A, which is used to make epoxy and other resins.

There are several types of phenolic micropollutants, including chloro, bromo, nitro, and alkyl phenol. Due to their toxicity and persistence in the environment, these phenolic compounds are listed as dangerous substances by the US Environmental Protection Agency (EPA). If these compounds are discharged without treatment, they may pose serious health risks to humans, animals, and aquatic systems. For a sustainable environment, phenol discharge limits have been set by international regulatory bodies. The EPA has established a water purity standard of less than 1 ppb for phenol in surface water [4]. For humans and aquatic life, toxicity levels are usually in the range of 9-25 mg/L [5]. As a disinfectant, phenyl phenols and bisphenols are widely used in hospitals and households. Furthermore, they are used in the textile and paper industry as well as cosmetics and leather. A wide range of applications caused these compounds to be found in a variety of parts of the environment, including surface water, sewage sludge, and marine sediments [6]. It was reported that these compounds exert estrogenic effects when exposed to the endocrine system. All of these phenolic compounds can cause both acute and chronic health effects. As phenols accumulate in the body, they can cause irregular breathing, muscle weakness, and respiratory arrest in humans at lethal doses. Additionally, chronic exposure to phenols causes irritation of the digestive system and the central nervous system in the liver, as well as growth retardation and abnormal development in animals.

Consequently, removing the phenols from industrial effluents water before entering a stream is highly recommended [7]. According to US EPA regulations, wastewater should not contain more than 1 mg/L of phenol [8]. Such contaminated drinking water damages the central nervous system, kidneys, liver, and pancreas when consumed by the human body [9, 10].

There are several methods for removing phenols, containing membrane filtration [11], adsorption [7, 12, 13], biological degradation [14], electrochemical oxidation [15]. Waste effluents can be effectively removed from organic matter using adsorption technology.

Surface adsorption occurs when a molecule is transferred from a fluid bulk to a solid surface. A chemical bond or physical force may be responsible for the process.The process is usually reversible (the reverse is called desorption); then it is responsible for both subtraction and release. A process such as this is described at the equilibrium using equations that determine the amount of material attached to the surface based on the fluid's concentration [16]. It is called an isotherm (the most famous are Langmuir and Freundlich equations) because their parameters are influenced by the temperature, which is one of the most significant environmental factors for adsorption. Ecological adsorption plays a vital role: It regulates the exchanges between the geosphere, hydrosphere, and atmosphere, controls the transport of substances within ecosystems, and triggers other important processes such as ionic exchange and enzymatic reactions. The most common adsorbent material used in wastewater treatment is activated carbon, which can be manufactured by pyrolyzing almost all carbonaceous organic materials, such as coal, wood, husks, coconut husks, and walnut shells. Its abundant microporous structure, large surface area, and high hydrophobicity make activated carbon an excellent adsorbent for most pollutants [17]. As adsorbents, activated carbons are widely used because they adsorb organic pollutants. The high initial cost of the material and the need for expensive regeneration make it not economic as an adsorbent. Okolo et al. [18] investigated phenol/chlorophenol's interaction with synthetic zeolites and determined that phenol has a 0.8 mmol/g adsorption capacity. New adsorbent materials have been proposed to replace activated carbon in order to enhance adsorption technology's practical application advantages. These include carbon-based adsorbents, nanoadsorbents, metal oxides,

and hydroxides-based adsorbents, resins, and modified or composite adsorbents.

MOFs, the uniform framework formed from inorganic and organic building blocks [19-21] with large porosities, high specific surface areas, open metal sites and ordered pore structures. The application orientations of MOFs in comparison to other adsorbents differ in that they have been evaluated in adsorptive separations in both gas and liquid phases with significant advantages, leading to advancement in making hierarchical pores or adding metals to MOFs [22-25].

MOFs (metal-organic frameworks) are crystalline materials with infinite network structures, exhibiting significant porosity and a large internal surface area. The network flexibility of MOFs is excellent, and they are closely related to coordination bonds, noncovalent bonds, and weak interactions, so they are useful in a number of areas. While MOFs possess many advantages, many of them are limited due to poor light and water resistance, poor mechanical strength, poor electrical conductivity, and vulnerability to degradation at ambient temperatures. By improving their properties and adding new functionality, MOFs will become more versatile and more applicable to realistic applications [26]. Therefore, it is suggested to combine MOFs with a wide range of functional materials to combine their merits and eliminate their weaknesses. A variety of MOFs and MOF composites are used for a variety of applications, such as gas storage, separation of hazardous chemicals, photocatalysis, sensing, drug delivery, biosensing, and sensing of certain substances. Among other subclasses of MOFs, zeolitic imidazolate frameworks (ZIFs) represent the highest chemical and thermal stability. In the class of metal-organic frameworks (MOFs) called zeolitic imidazolate frameworks (ZIFs), metal-organic frameworks with topologically similar structures to zeolites have been studied. ZIFs are made of tetrahedra-coordinated transition metal ions (e.g. Fe, Co, Cu, Zn) linked by imidazolate linkers. ZIFs exhibit a zeolite-like structure since the metal-imidazole-metal angle is similar to the 145° Si-O-Si angle in zeolites. A ZIF can be used to capture carbon dioxide because of its robust porosity, resistance to thermal changes, and chemical stability [27]. Additionally, ZIF-8 has shown great promise as a heterogeneous catalyst; it can easily catalyze the transesterification of vegetable oils, the Friedel-Crafts acylation of benzoyl chloride and anisole, and the formation of carbonates. Nanoparticles of ZIF-8 can also be used to enhance the performance of the Knoevenagel reaction between benzaldehyde and malononitrile. ZIF-8 also has low coordination Zn sites and a large surface area, making it an ideal adsorbent for mercaptans [28-31].

This study reports the facile synthesis of Ni/ZIF-8 for adsorptive removal and its characterization with XRD, FE-SEM, FTIR and BET. Among zeolite-like MOFs, ZIF-8 was screened for its ability to remove nitrogen compounds due to the presence of nitrogen compounds. The effects of operating conditions on the adsorptive process were analyzed using adsorption isotherms studies to understand phenol's interactions with the framework fully.

2. Materials and methods

2.1. Synthesis of Ni-doped ZIF-8

To prepare Ni-doped ZIF-8, 40 ml of deionized water were combined with nickle (II) nitrate and zinc nitrate tetrahydrate (total 0.02 mol, molar ratio of 1:2 Zn/M). $Zn(NO_3)2.4H_2O$ and specific metal salts were then combined with 2-methylimidazolate solution (HMeIM) (0.07 mol in 40 mL of DW) at 25°C. The N-butyl amine was then poured gradually into the as-prepared mixture while stirring at 50°C, and the pH was checked to ensure it reached 9. Afterward, the mixture was moved to a 200-mL autoclave and heated to 140°C for 18 hours. The Ni-doped ZIF-8 crystals were then washed several times. As a first step in the adsorptive reaction, the prepared samples were heated to 110°C in a programmable oven for 18 hours under vacuum conditions and

then allowed to cool to 25°C. Before use, the Ni-doped ZIF-8 powders were tightly sealed and stored at 25°C.

2.2. Characterization techniques

The X-ray diffraction analysis was applied at 25 °C using an X'Pert PRO X-ray diffractometer (B.V., Netherlands). The sizes and morphology of the products were determined by scanning electron microscopy with the Sirion 200 field emission scanning electron microscope. A Quantachrome ChemBET-3000 instrument was applied to calculate the BET surface area with N2 adsorption at -196 °C. A Nicolet 370 spectrophotometer was used for diffuse reflectance FTIR. Under flow of nitrogen, FTIR experiments on heat-treated samples were carried out on pure powder samples without KBr.

2.3. Adsorption experiments

The batch method was applied to investigate the adsorption isotherms of phenol (from Fluka) at pH= 5. The C_6H_5OH solutions were obtained in 0.15 M NaCl. Using Metrohm, 0.06 M HCl/0.05 M NaOH solutions were applied to change the solutions pH. A solution of phenol adsorbate was added in equal parts to a solution of 0.15 g adsorbent in 300mL-stoppered Erlenmeyer flasks. The samples were taken over 18 hours (during which portions of each solution were diluted to 20 mL by adding 0.15 M NaCl solution). In both the solutions before and after adsorption, the phenol concentration was determined with a UV/vis spectrophotometer at λ = 270 nm. A batch setup was used in which three replicates were carried out and average values and deviations were reported. The following adsorption capacities (q_e, mmol g^{-1}) were calculated:

$$q_e = \frac{C_0 - C_e}{m} V \tag{1}$$

The initial and equilibrium metal ion concentrations are represented by C_0 and C_e (mM), respectively. The percent removal of phenol (%*R*) was determined using the equation [32]:

$$\%R = \frac{(C_0 - C_e)}{C_0} \times 100 \tag{2}$$

A dilute solution of NaOH or HCl was also added to set the pH of the solution using a pH meter with a resolution of ±0.05. Experiments were conducted in triplicate, with average values reported.

3. Results and discussion

3.1. Characterization

Fig. 1 indicates the XRD patterns of ZIF-8 and Ni-doped ZIF-8 samples. According to ZIF-8, the XRD patterns of modified crystals are consistent with same structure. Some of the extra peaks shown in Fig. 1 of the XRD pattern of Ni/ZIF-8 are likely to be NiHMeIM clusters formed when Ni^{2+} ions and HMeIM are trapped in ZIF-8 cavities [33]. In addition, it is important to note that Ni^{2+} ions have been shown to cause crystallinity damage to ZIF-8 once they are added to these nanocrystals due to their interactions with the HMeIM- linkers. FE-SEM images reveal two distinct microscopical morphologies, suggesting Ni-HMeIM nanosphere clusters ranging from 85–95 nm are formed in ZIF-8 pores.

Ni/ZIF-8 samples were characterized by N_2 adsorption in terms of surface area and porosity. For Ni/ZIF-8 and pristine ZIF-8, the type-I isotherms suggested that the samples were

microporous. The BET surface areas for these samples were 623 m^2g^{-1} and 1058 m^2g^{-1}, respectively. The size distribution analysis shows that most of Ni/ZIF-8's pores are micro, meso-sized pores. Micropore volumes and surface areas and are similar to those of pure ZIF-8 (S_{BET} = 1058 m^2g^{-1} and V_{micro} = 0.44 cm^3 g^{-1}) in Table 1.

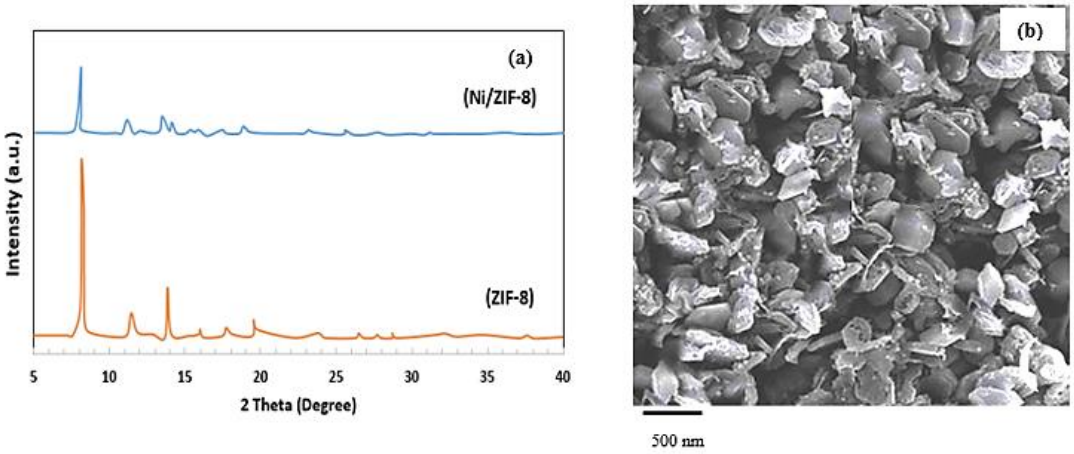

Fig. 1. (a) XRD patterns of ZIF-8 and Ni-doped ZIF-8 crystals, and (b) FE-SEM images of Ni/ZIF-8 crystals

Furthermore, the pore volume of nanocrystals synthesized with Ni doping (0.38 compared to 0.44 in pristine ZIF-8) was slightly reduced. Furthermore, the results show that Ni-HMeIM clusters occupy some cages in Ni/ZIF-8.

Table 1. Textural properties of obtained samples

Sample	BET surface area (m^2g^{-1})	Total Pore volume (cm^3 g^{-1})	Small pore size (nm)
ZIF-8	1058	0.44	1.22
Ni/ZIF-8	623	0.38	1.58

FITR was used to define the chemical structure shown in Fig. 2. The ZIF-8 sample showed remarkable bands at 3460, 3142, 2933, 1641, 1592, 1419, 1391, 998, 757, 689 and 431 cm^{-1}. The FT-IR bands were consistent with those previously reported by Ordonez et al. [34]. The band at 3460 cm^{-1} may result from the N-H vibration of residual Hmim and the O-H vibration of water from KBr deliquescence. Asymmetry stretching vibrations in aromatic and aliphatic C–H atoms, respectively, were associated with peaks at 3142 and 2933 cm^{-1}. An additional signal at 1635 cm^{-1} arose from the C=C stretch mode, while the 1592 cm^{-1} band reflected the C=N stretch vibration. The signals at 1300–1460 cm^{-1} are from stretching of the entire ring, whereas the signals at 1146 $cm^{-1}$are from aromatic C–N stretching. The peaks at 998 and 757 cm^{-1} could be classified as vibration modes for C–N bending and C–H bending, respectively. Zn–N stretching vibrations were observed at 426 cm^{-1} position, indicating that zinc ions combined chemically with nitrogen atoms of the methylimidazole groups to form imidazolates. Ni/ZIF-8 sample did not show any new bands. The results showed that no strong chemical interactions occurred between ZIF-8 particles and Ni.

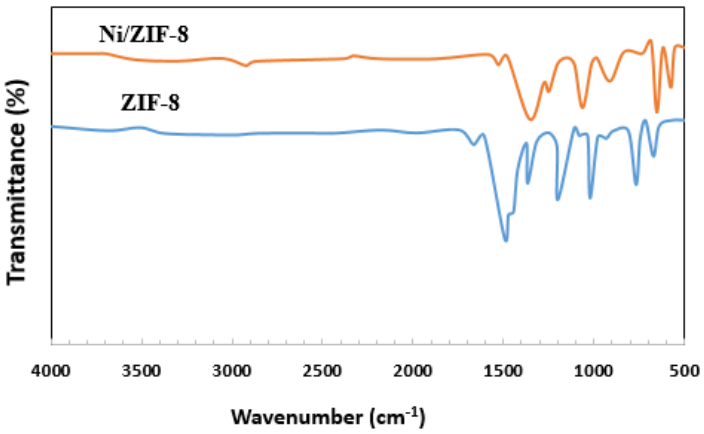

Fig. 2. The FT-IR spectra of ZIF-8 and Ni/ZIF-8

3.2. Effect of Operating Parameters

Temperature considerably influences the adsorption efficiency of Ni/ZIF-8. The phenol uptake onto Ni/ZIF-8 adsorbent, q_e (mg/g), is plotted against the solution temperature after 24 hours in Fig. 3. The phenol uptake decreased from 25 to 60°C, especially for more concentrated solutions. Adsorption is proven to be exothermic by these results.

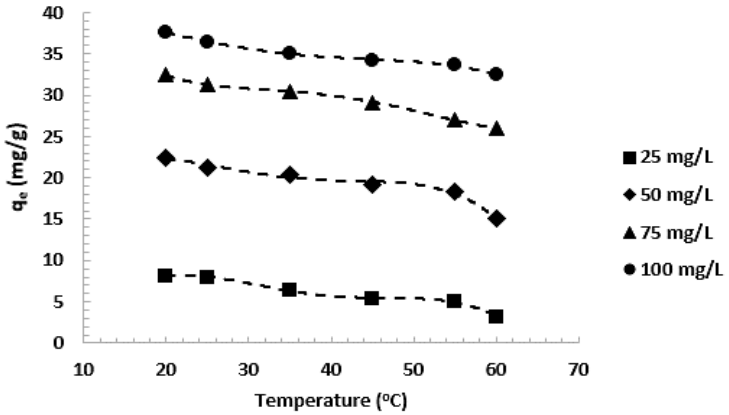

Fig. 3. Effect of solution temperature on phenol uptake

To measure the equilibrium time, phenol was adsorption studied at various initial concentrations on Ni/ZIF-8 as a function of contact time. Fig. 4 indicates the effect of the time on the phenol removal at 30 °C. Adsorption uptake is rapid and increases with increasing time. At the equilibrium point, there was a dynamic equilibrium between the C_6H_5OH amount being absorbed and desorbing from the adsorbent. Based on the operating conditions applied, the C_6H_5OH quantity adsorbed at equilibrium corresponded to the adsorbent's maximum uptake during adsorption. The results indicate that adsorption reaches equilibrium earlier.

In the beginning, there are numerous vacant surface sites that are available for adsorption. This occurs at a very fast rate, resulting in a rapid accumulation of adsorbates on the Ni/ZIF-8 surface after 4 h. During this period, the adsorption uptake for 25, 50, 75,

and 100 mg/L phenol solutions was 92%, 83%, 78%, and 86%, respectively. As reported [33], the remaining vacant sites on surfaces cannot be occupied because of the repulsion between C_6H_5OH molecules (on surfaces and in bulk). Eventually, these led to a decrease in adsorption rate, which was confirmed by the plateau line after 7 hours of adsorption, showing that the process has reached steady state [35]. In a concentration range from 25 to 100 mg/L, qe increases from 18.4 to 28.6 mg/g as the initial concentration increases. Other temperatures showed similar adsorption trends. To ensure equilibrium, all adsorption isotherms were studied at a contact time of 24 h. Longer contact times were avoided to prevent the dissolution of the adsorbent.

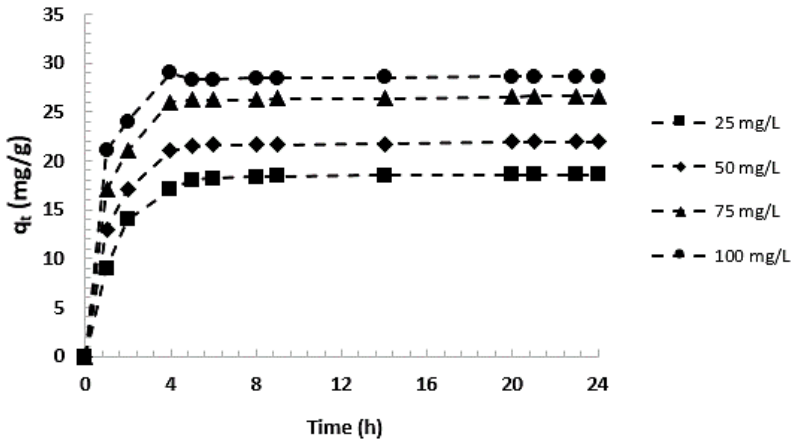

Fig. 4. The effect of contact time on phenol adsorption onto Ni/ZIF-8 at 30 °C.

3.3. Adsorption Isotherm and Kinetics

Understanding the equilibrium isotherm is very important when studying adsorption systems. Adsorption isotherms are a function of solute concentration and amount constant at a given temperature [36, 37]. The process provides crucial physiochemical data for measuring the feasibility of the entire process. Experimental adsorption equilibrium data can be analyzed using several isotherm equations [38]. In Langmuir's model, adsorption takes place in monolayers, and the assumption is that the adsorbent surface contains an even number of active sites, and, therefore, a constant adsorption energy [39]. The Langmuir adsorption isotherm expression is represented by the Eq. (3) [40]:

$$q_e = \frac{q_{max} K_L C_e}{1 + K_L C_e} \tag{3}$$

The Langmuir adsorption constants q_{max} (mg/g) and K_L (L/mg) show the capacity and speed of adsorption, respectively, based on the amount of phenol adsorbed per unit mass of adsorbent. According to Freundlich, the surface energy of the adsorbent is heterogeneous, in contrast to Langmuir. With increasing site occupation, the binding strength decreases [41]. Binding sites with the strongest affinity are occupied first. Eq. (4) shows the Freundlich adsorption isotherm [42]:

$$q_e = K_F C_e^{1/n} \tag{4}$$

K_F is the adsorption capacity. 1/n is a dimensionless measure of either surface heterogeneity or adsorption intensity. It ranges from zero to one. Adsorbent-adsorbate interactions are explicitly considered in the Temkin isotherm model [43]. Due to the interactions between adsorbent and adsorbate, adsorption heat would decrease linearly with coverage for all molecules in the layer. As adsorption progresses, binding energies increase uniformly until a maximum is reached [44]. Temkin's isotherm is shown in Eq. (4) [45]:

$$q_e = \frac{RT}{b_T} \ln (A_T C_e) \quad (5)$$

A_T (L/g) is the equilibrium binding constant related to the maximum binding energy, B (=RT/b_T) is the Temkin constant related to the adsorption heat, C_e (mg/L) is the equilibrium concentration of phenol. Table 2 provides the Langmuir parameters (K_L and q_{max}), Freundlich parameters (K_F and n), and Temkin parameters (A_T and B_T).

Table 2. Isotherm model parameters of phenol adsorption onto Ni/ZIF-8

Model	Parameters	T=25 °C	T=40 °C	T=60 °C
Langmuir	q_{max} (mg/g)	36.8	25.9	22.4
	K_L (L/mg)	0.47	0.27	0.25
	R^2	0.965	0.972	0.974
Freundlich	K_F (mg/g (L/mg)$^{1/n}$)	11.26	10.48	9.25
	n	3.24	4.62	3.38
	R^2	0.982	0.973	0.942
Temkin	A_T (L/g)	15.62	12.48	5.85
	B	4.83	2.64	3.26
	R^2	0.924	0.937	0.928

Because of the highest R^2 values listed and in Table 3, the Freundlich model provided the best fit at temperatures 25 and 40°C (R^2 > 0.97). Therefore, the Freundlich isotherm is the best equation to characterize the equilibrium adsorption onto Ni/ZIF-8. 1/n represents a favorable adsorption. The Langmuir model fitted the experimental data well, with qm, 36.8, 25.9 and 22.4 mg/g at temperatures 25, 40, and 60°C. According to the model's applicability, the adsorbate surfaces of the adsorbent will be covered by monolayers. Based on the Temkin isotherm equations (R^2 = 0.92–0.94), the determination coefficients are extremely low, so they cannot adequately represent experimental data.

Adsorption kinetics plays an important role in explaining adsorption's effectiveness. Wilczak and Keinath [46] and Chiron et al. [47] used double-exponential models to study the adsorption kinetics of asphaltene on nanocomposites. Below is the double-exponential model:

$$q_t = q_e - \frac{D_1}{m_a} \exp(-K_{D_1} t) - \frac{D_2}{m_a} \exp(-K_{D_2} t) \quad (6)$$

Asphaltene adsorbed at equilibrium time (q_e) and at time t (q_t), respectively, are represented by mg.g^{-1}. D_1 and D_2 (mg/L) are the adsorption rate parameters, K_{D1} and K_{D2} (h^{-1}) are the mass transfer coefficients, and m_a is the amount of the adsorbent in the solution (g/L). Adsorption of asphaltene particles is controlled by mass transfer diffusion in two steps: fast and slow. The parameters with subscripts 1 and 2 represent the fast and slow steps, respectively, in a double-exponential model.

The first stage of adsorption is characterized by rapid adsorption with external and internal diffusion that takes place in a few minutes. In the second stage, the adsorption is slower and eventually reaches equilibrium.

The data shows that the double-exponential model is very close to the experimental findings, and this model can explain the asphaltene adsorption kinetics on Ni/ZIF-8, which indicates that the process is chemical. According to the data, the double-exponential model accurately predicts the phenol adsorption kinetics on Ni/ZIF-8 and this model is useful to understand the phenol adsorption process, indicating that this is a chemical adsorption process. As a result of the experiments, phenol adsorption on Ni/ZIF-8 occurs faster at high initial concentrations. Thus, the Ni/ZIF-8 phenol adsorption operation achieves equilibrium at very high initial concentrations.

3.4. Adsorption Thermodynamic

The adsorption standard free energy changes (ΔG^0) can be calculated as follows:

$$\Delta G^0 = -RT\ ln\ K_0 \tag{7}$$

R denotes the universal gas constant (1.98 cal/deg/mol) and T its temperature in kelvins. Van't Hoof's equation gives the average standard enthalpy change (ΔH^0) [48].

$$ln\ K_0\ (T_3) - ln\ K_0\ (T_1) = \frac{-\Delta H^0}{R}\ (\frac{1}{T_3} - \frac{1}{T_1}) \tag{8}$$

T_3 and T_1 represent two different temperatures. Standard entropy change (ΔS^0) can be calculated by

$$\Delta G^0 = -\frac{\Delta G^0 - \Delta H^0}{T} \tag{9}$$

Table 3 lists the thermodynamic parameters. Positive standard enthalpy changes suggest that phenol is endothermic when adsorbed by Ni/ZIF-8, as indicated by the increasing adsorption of phenol as temperature increases; a positive standard entropy change and a negative adsorption free energy change indicate that the adsorption reaction is spontaneous [49]. This positive standard entropy change may result from the release of water molecules due to the ion exchange reaction between the adsorbate and the functional groups on the surfaces of the adsorbent [50].

Table 3. Values of various thermodynamic parameters for adsorption of phenol on Ni/ZIF-8.

Thermodynamic constants	Temperature (°C)		
	25	40	60
K_0	11.62	12.25	12.48
$\Delta G^0 \times 1000\ cal\ mol^{-1}$	-1.45	-1.52	-1.58
$\Delta H^0 \times 1000\ cal\ mol^{-1}$	0.45	0.47	0.47
$\Delta S^0 \times 1000\ cal\ mol^{-1}$	6.25	6.32	6.28

4. Conclusions

Ni/ZIF-8 can be applied as a promising material for removing phenol from water in the present study. According to adsorption kinetics, C_6H_5OH adsorption does not depend on intraparticle diffusion. The adsorption of phenol decreased with increasing temperature in the range of 25-60°C. At 25 to 60°C, Freundlich models modeled the equilibrium data best, whereas the Langmuir model modeled it best at 60°C. Positive values of enthalpy change indicate endothermy in the interaction between Ni/ZIF-8 and phenol adsorbed. In addition to the negative adsorption standard free energy changes, the positive standard entropy changes indicate that the adsorption reaction is spontaneous.

References

1. Sedighi M, Mohammadi M, (2018). Application of green novel NiO/ZSM-5 for removal of lead and mercury ions from aqueous solution: investigation of adsorption parameters. Journal of Water and Environmental Nanotechnology, pp: 3: 301-310.
2. Lee C-G, Hong S-H, Hong S-G, Choi J-W, Park S-J, (2019). Production of biochar from food waste and its application for phenol removal from aqueous solution. Water, Air, & Soil Pollution, pp: 230: 1-13.
3. Emamjomeh M M, Mousazadeh M, Mokhtari N, Jamali H A, Makkiabadi M, Naghdali Z, Hashim K S, Ghanbari R, (2020). Simultaneous removal of phenol and linear alkylbenzene sulfonate from automotive service station wastewater: Optimization of coupled electrochemical and physical processes. Separation Science and Technology, pp: 55: 3184-3194.
4. Kazemi P, Peydayesh M, Bandegi A, Mohammadi T, Bakhtiari O, (2014). Stability and extraction study of phenolic wastewater treatment by supported liquid membrane using tributyl phosphate and sesame oil as liquid membrane. Chemical engineering research and design, pp: 92: 375-383.
5. Sharma S, Bhattacharya A, (2017). Drinking water contamination and treatment techniques. Applied water science, pp: 7: 1043-1067.
6. Olak M, Gmurek M, Miller J S, (2012). Phenolic compounds in the environment-occurrence and effect on living organisms. Proceedings of ECOpole, pp: 6:
7. Lütke S F, Igansi A V, Pegoraro L, Dotto G L, Pinto L A, Cadaval Jr T R, (2019). Preparation of activated carbon from black wattle bark waste and its application for phenol adsorption. Journal of Environmental Chemical Engineering, pp: 7: 103396.
8. Banat F, Al-Bashir B, Al-Asheh S, Hayajneh O, (2000). Adsorption of phenol by bentonite. Environmental pollution, pp: 107: 391-398.
9. Zhang D, Huo P, Liu W, (2016). Behavior of phenol adsorption on thermal modified activated carbon. Chinese Journal of Chemical Engineering, pp: 24: 446-452.
10. Sedighi M, Ghasemi M, Sadeqzadeh M, Hadi M, (2016). Thorough study of the effect of metal-incorporated SAPO-34 molecular sieves on catalytic performances in MTO process. Powder Technology, pp: 291: 131-139.
11. Zagklis D P, Vavouraki A I, Kornaros M E, Paraskeva C A, (2015). Purification of olive mill wastewater phenols through membrane filtration and resin adsorption/desorption. Journal of hazardous materials, pp: 285: 69-76.

12. Suzuki H, Araki S, Yamamoto H, (2015). Evaluation of advanced oxidation processes (AOP) using O3, UV, and TiO2 for the degradation of phenol in water. Journal of Water Process Engineering, pp: 7: 54-60.
13. Fu Y, Shen Y, Zhang Z, Ge X, Chen M, (2019). Activated bio-chars derived from rice husk via one-and two-step KOH-catalyzed pyrolysis for phenol adsorption. Science of the Total Environment, pp: 646: 1567-1577.
14. Basha K M, Rajendran A, Thangavelu V, (2010). Recent advances in the biodegradation of phenol: a review. Asian J Exp Biol Sci, pp: 1: 219-234.
15. Enache T A, Oliveira-Brett A M, (2011). Phenol and para-substituted phenols electrochemical oxidation pathways. Journal of Electroanalytical Chemistry, pp: 655: 9-16.
16. Al-Ghouti M A, Da'ana D A, (2020). Guidelines for the use and interpretation of adsorption isotherm models: A review. Journal of hazardous materials, pp: 393: 122383.
17. Ugwu E I, Agunwamba J C, (2020). A review on the applicability of activated carbon derived from plant biomass in adsorption of chromium, copper, and zinc from industrial wastewater. Environmental monitoring and assessment, pp: 192: 1-12.
18. Okolo B, Park C, Keane M A, (2000). Interaction of phenol and chlorophenols with activated carbon and synthetic zeolites in aqueous media. Journal of colloid and interface science, pp: 226: 308-317.
19. Wang S, McGuirk C M, d'Aquino A, Mason J A, Mirkin C A, (2018). Metal–organic framework nanoparticles. Advanced Materials, pp: 30: 1800202.
20. Bahrami H, Darian J T, Sedighi M, (2018). Simultaneous effects of water, TEAOH and morpholine on SAPO-34 synthesis and its performance in MTO process. Microporous and Mesoporous Materials, pp: 261: 111-118.
21. Sedighi M, Towfighi J, Mohamadalizadeh A, (2014). Effect of phosphorus and water contents on physico-chemical properties of SAPO-34 molecular sieve. Powder technology, pp: 259: 81-86.
22. Li W, Cao J, Xiong W, Yang Z, Sun S, Jia M, Xu Z, (2020). In-situ growing of metal-organic frameworks on three-dimensional iron network as an efficient adsorbent for antibiotics removal. Chemical Engineering Journal, pp: 392: 124844.
23. Li D, Tian X, Wang Z, Guan Z, Li X, Qiao H, Ke H, Luo L, Wei Q, (2020). Multifunctional adsorbent based on metal-organic framework modified bacterial cellulose/chitosan composite aerogel for high efficient removal of heavy metal ion and organic pollutant. Chemical Engineering Journal, pp: 383: 123127.
24. Parmar B, Bisht K K, Rajput G, Suresh E, (2021). Recent advances in metal–organic frameworks as adsorbent materials for hazardous dye molecules. Dalton Transactions, pp: 50: 3083-3108.
25. Ghasemi M, Mohammadi M, Sedighi M, (2020). Sustainable production of light olefins from greenhouse gas CO2 over SAPO-34 supported modified cerium oxide. Microporous and Mesoporous Materials, pp: 297: 110029.

26. Kirchon A, Feng L, Drake H F, Joseph E A, Zhou H-C, (2018). From fundamentals to applications: a toolbox for robust and multifunctional MOF materials. Chemical Society Reviews, pp: 47: 8611-8638.
27. Dai H, Yuan X, Jiang L, Wang H, Zhang J, Zhang J, Xiong T, (2021). Recent advances on ZIF-8 composites for adsorption and photocatalytic wastewater pollutant removal: Fabrication, applications and perspective. Coordination Chemistry Reviews, pp: 441: 213985.
28. Hoop M, Walde C F, Riccò R, Mushtaq F, Terzopoulou A, Chen X-Z, deMello A J, Doonan C J, Falcaro P, Nelson B J, (2018). Biocompatibility characteristics of the metal organic framework ZIF-8 for therapeutical applications. Applied Materials Today, pp: 11: 13-21.
29. Krokidas P, Moncho S, Brothers E N, Castier M, Economou I G, (2018). Tailoring the gas separation efficiency of metal organic framework ZIF-8 through metal substitution: A computational study. Physical Chemistry Chemical Physics, pp: 20: 4879-4892.
30. Li S, Wei X, Zhu S, Zhou Q, Gui Y, (2021). Adsorption behaviors of SF6 decomposition gas on Ni-doped ZIF-8: A first-principles study. Vacuum, pp: 187: 110131.
31. Sedighi M, Mohammadi M, (2020). CO2 hydrogenation to light olefins over Cu-CeO2/SAPO-34 catalysts: Product distribution and optimization. Journal of CO2 Utilization, pp: 35: 236-244.
32. Safari M, Mohammadi M, Sedighi M, (2017). Effect of neglecting geothermal gradient on calculated oil recovery. Journal of Applied Geophysics, pp: 138: 33-39.
33. Kaur G, Rai R K, Tyagi D, Yao X, Li P-Z, Yang X-C, Zhao Y, Xu Q, Singh S K, (2016). Room-temperature synthesis of bimetallic Co–Zn based zeolitic imidazolate frameworks in water for enhanced CO 2 and H 2 uptakes. Journal of Materials Chemistry A, pp: 4: 14932-14938.
34. Ordonez M J C, Balkus Jr K J, Ferraris J P, Musselman I H, (2010). Molecular sieving realized with ZIF-8/Matrimid® mixed-matrix membranes. Journal of Membrane Science, pp: 361: 28-37.
35. Bhatnagar A, (2007). Removal of bromophenols from water using industrial wastes as low cost adsorbents. Journal of Hazardous Materials, pp: 139: 93-102.
36. Mohammadi M, Safari M, Ghasemi M, Daryasafar A, Sedighi M, (2019). Asphaltene adsorption using green nanocomposites: Experimental study and adaptive neuro-fuzzy interference system modeling. Journal of Petroleum Science and Engineering, pp: 177: 1103-1113.
37. Mohammadi M, Sedighi M, Hemati M, (2020). Removal of petroleum asphaltenes by improved activity of NiO nanoparticles supported on green AlPO-5 zeolite: Process optimization and adsorption isotherm. Petroleum, pp: 6: 182-188.
38. Mohammadi M, Sedighi M, Ghasemi M, (2021). Systematic investigation of simultaneous removal of phosphate/nitrate from water using Ag/rGO nanocomposite: Development, characterization, performance and mechanism. Research on Chemical Intermediates, pp: 47: 1377-1395.
39. Bergaoui M, Nakhli A, Benguerba Y, Khalfaoui M, Erto A, Soetaredjo F E, Ismadji S, Ernst B, (2018). Novel insights into the adsorption mechanism of methylene blue onto organo-

bentonite: Adsorption isotherms modeling and molecular simulation. Journal of molecular liquids, pp: 272: 697-707.
40. Mohammadi M, Sedighi M, (2013). Modification of Langmuir isotherm for the adsorption of asphaltene or resin onto calcite mineral surface: Comparison of linear and non-linear methods. Protection of Metals and Physical Chemistry of Surfaces, pp: 49: 460-470.
41. Mohammadi M, Shahrabi M A, Sedighi M, (2012). Comparative study of linearized and non-linearized modified Langmuir isotherm models on adsorption of asphaltene onto mineral surfaces. Surface Engineering and Applied Electrochemistry, pp: 48: 234-243.
42. Fan C, Zhang Y, (2018). Adsorption isotherms, kinetics and thermodynamics of nitrate and phosphate in binary systems on a novel adsorbent derived from corn stalks. Journal of Geochemical Exploration, pp: 188: 95-100.
43. Mohammadi M, Sedighi M, Alimohammadi V, (2019). Modeling and optimization of Nitrate and total Iron removal from wastewater by TiO2/SiO2 nanocomposites. International Journal of Nano Dimension, pp: 10: 195-208.
44. Mohammadi M, Sedighi M, Natarajan R, Hassan S H A, Ghasemi M, (2021). Microbial fuel cell for oilfield produced water treatment and reuse: Modelling and process optimization. Korean Journal of Chemical Engineering, pp: 38: 72-80.
45. Mohammed B B, Yamni K, Tijani N, Alrashdi A A, Zouihri H, Dehmani Y, Chung I-M, Kim S-H, Lgaz H, (2019). Adsorptive removal of phenol using faujasite-type Y zeolite: adsorption isotherms, kinetics and grand canonical Monte Carlo simulation studies. Journal of Molecular Liquids, pp: 296: 111997.
46. Wilczak A, Keinath T M, (1993). Kinetics of sorption and desorption of copper (II) and lead (II) on activated carbon. Water Environment Research, pp: 65: 238-244.
47. Chiron N, Guilet R, Deydier E, (2003). Adsorption of Cu (II) and Pb (II) onto a grafted silica: isotherms and kinetic models. Water Research, pp: 37: 3079-3086.
48. Shamshiri A, Alimohammadi V, Sedighi M, Jabbari E, Mohammadi M, (2020). Enhanced removal of phosphate and nitrate from aqueous solution using novel modified natural clinoptilolite nanoparticles: process optimization and assessment. International Journal of Environmental Analytical Chemistry, pp: 1-20.
49. Niwas R, Gupta U, Khan A, Varshney K, (2000). The adsorption of phosphamidon on the surface of styrene supported zirconium (IV) tungstophosphate: a thermodynamic study. Colloids and Surfaces A: Physicochemical and Engineering Aspects, pp: 164: 115-119.
50. Liang R, Chen B, (2004). Study of the effects of ionic strength and temperature on the adsorption of anionic dye on activated carbon with flow injection-spectrophotometry. Chem. Bull, pp: 67: 1-8.